

# MECHANICAL PROPERTIES OF BASALT: A STUDY ON COMPRESSIVE LOADING AT DIFFERENT STRAIN RATES USING SHPB

JAN FALTA<sup>a,\*</sup>, NELA KRČMÁŘOVÁ<sup>a</sup>, TOMÁŠ FÍLA<sup>a</sup>, MARTIN VAVRO<sup>b</sup>,  
LEONA VAVRO<sup>b</sup>

<sup>a</sup> Czech Technical University in Prague, Faculty of Transportation Sciences, Department of Mechanics and Materials, Konviktská 20, 110 00 Prague 1, Czech Republic

<sup>b</sup> Czech Academy of Sciences, Institute of Geonics, Studentská 1768/9, 708 00 Ostrava-Poruba, Czech Republic

\* corresponding author: [falta@fd.cvut.cz](mailto:falta@fd.cvut.cz)

**ABSTRACT.** This article focuses on the mechanical properties of basalt in compressive loading at different strain-rates. The study employs advanced instrumentation for the evaluation of the results in dynamic conditions, while standard uni-axial loading device is used for evaluation in quasi-static conditions. Basalt specimens were subjected to four different loading-rates from 200–600 s<sup>-1</sup> on which the stress-strain dependence was evaluated together with DIC analysis of crack initiation and disintegration process. Understanding the mechanical properties of basalt can provide insights for engineers and designers in creating structures that are durable and able to withstand different loading conditions. The findings of this study can have implications for a wide range of industries, including aerospace, automotive, and construction, among others.

**KEYWORDS:** SHPB, basalt, compressive loading, dynamic loading.

## 1. INTRODUCTION

Basalt is an igneous rock that is highly versatile in a range of applications. Basalt's high strength and non-corrosive properties make it a suitable material for reinforced concrete structures in specific environments [1]. Basalt fibers can be also used as a reinforcing material in composites for various industrial applications [2]. Cement-based composites, particularly concrete, are widely used in the construction industry [3, 4]. They play a crucial role in building structures like highway bridges, tunnels, and dams, intended to endure for many generations. However, these structures often exhibit nonlinear behavior under loading, specifically quasi-brittle characteristics. Even after deviating from the linear force-displacement diagram, they can still bear loads until reaching a peak point. Subsequently, a decline in loading force occurs, ultimately leading to failure a phenomenon referred to as tensile softening [5]. This behavior can be attributed to various factors such as the presence of internal defects (e.g., pores, cracks, transition zones) or material discontinuities (e.g., inclusions for example olivine, labradorite, magnetite, nepheline) that act as obstacles or facilitators for crack propagation. Surprisingly, existing standards, such as EN 1992-1-1 (2004), completely overlook these stress concentrators, which have the potential to serve as weak elements within the composites. The aim of this work is to reveal the influence of compressive loading at different strain-rates on the mechanical response of the basalt rock and to inspect the failure mechanism of the sample using digital image correlation.

## 2. MATERIALS AND METHODS

### 2.1. MATERIAL CHARACTERIZATION OF THE BÍLČICE BASALT

Olivine basalt to nepheline basanite used in the experiment came from the active Bílčice quarry (approx. 12 km SE from the city of Bruntál and near the ride side of the Slezská harta dam). The rock deposit is situated in the SE edge of the Chříbský les stream, which represents the largest of the four known lava streams of the Velký Roudný stratovolcano.

The quarried Plio-Pleistocene basaltoids are gray to black-gray volcanic rocks with a distinct porphyritic texture. From the structural point of view, two basic types of basaltoids are developed in the deposit: (1) predominant fine-grained, massive, compact, only in places porous basalt with block to tabular jointing, from which the test specimens were prepared; and (2) basalt with a typical orbicular structure with spherical (pea-like) disintegration and well-developed columnar jointing Figure 1. Rock phenocrysts are predominantly formed by green to green-yellow crystals of olivine (approx. 15–20% of the rock volume, max. 1–2% in size), clinopyroxene can occur only subsidiary. Rock matrix is composed of clinopyroxene (in particular augite, approx. 37–45% of the rock volume), calcium-rich plagioclase of labradorite composition (about 20–30%), magnetite (between 10 and 20%) and possibly also nepheline (up to 1%). The proportion of amorphous phase (basaltic glass) is up to 3% [6].

The Bílčice basalt under study exhibit a high bulk density, relatively low water absorption capacity and

Uniaxial compressive strength [MPa]	Fracture toughness [MPa m <sup>1/2</sup> ]	Ultrasonic wave velocity [km s <sup>-1</sup> ]	Splitting tensile strength [MPa]	Specific density [kg m <sup>-3</sup> ]	Total porosity [%]
232	3.09	5.49	12.3	3032	3.44

TABLE 1. Basic physical, mechanical and mechanical fracture properties of the Bílčice basalt.

total porosity, high values of P-wave velocity, and high to very high strength properties Table 1 [2]. These properties predetermine the Bílčice basalt as a source of high-quality crushed aggregate.



FIGURE 1. Typical columnar jointing visible in the Bílčice quarry wall.

## 2.2. SPECIMENS

In this study, samples drilled from a single piece of basalt, which you can see in Figure 2, were used. The samples are 20 mm long and 12 mm in diameter. A total of 17 specimens were tested, 5 pc under quasi-static loading (1 mm min<sup>-1</sup>), 5 pc tested dynamically in contact with an incident bar at a strain-rate of 200 s<sup>-1</sup>, 5 pc tested dynamically in contact with an incident bar at a strain-rate of 300 s<sup>-1</sup>, 1 pc by the impact of an incident bar at a strain-rate of 400 s<sup>-1</sup>, 1 pc by incident bar impact at strain-rate 600 s<sup>-1</sup>.

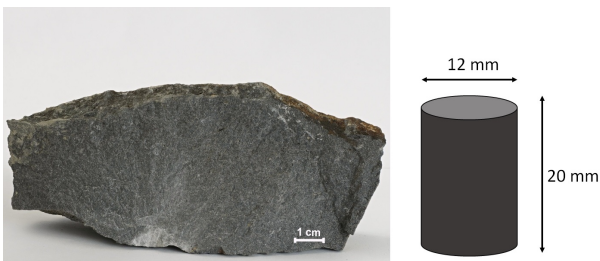


FIGURE 2. Macrophotograph of the massive type of the Bílčice basalt with illustration of one specimen.

## 2.3. EXPERIMENTAL SETUP

The mechanical response of the structures was investigated under dynamic conditions using a Split Hopkinson Pressure Bar (SHPB) apparatus equipped with strain gauges and a high-speed camera (Fastcam

SA-Z, Photron, Japan). The camera was set to capture frames at a rate of 300.000 fps with a resolution of 256 × 256 pixels. Figure 3 illustrates a diagram and schematic of the loading device.

The dynamic loading device comprised two bars: a striker bar housed within a gas-gun barrel and a transmission bar. Both bars had a uniform diameter of 20 mm and were constructed from a high-strength aluminum alloy (EN-AW-7075-T6). The striker bar was accelerated using a single-stage gas-gun, generating a strain pulse when the striker projectile impacted the front face of the incident bar. To shape the strain pulse, a cylindrical copper pulse shaper was placed on the front face of the incident bar.

Strain measurements were conducted using foil strain gauges (3/120 LY61, HBM, Germany) connected in a Wheatstone half-bridge configuration to compensate for any minor deflections in the bars. The data acquisition systems and cameras were triggered by a pair photoelectric sensors, enabling estimation of the impact velocity.

## 3. RESULTS

### 3.1. QUASI-STATIC LOADING

The mechanical response of the investigated structures to quasi-static uni-axial compressive loading was expressed by the average engineering stress-strain diagram from 5 tested specimens with standard deviation was evaluated. The maximum stress value was approx. 270 MPa at strain between 2.5–3.0%.

### 3.2. DYNAMIC LOADING

To reveal a possible strain-rate sensitivity of the deformation response, dynamic compression tests using the SHPB apparatus were conducted at four different loading-rates with two different loading conditions.

#### 3.2.1. INCIDENT BAR IN CONTACT WITH SPECIMEN

In this case, it was the standart placement of the specimen for the SHPB assembly, so that the specimen is sandwiched between the incident and transmission bars. For the first low-rate, the speed of the impactor was determined using a pair of short-reaction time through-beam optical gates (FS/FS 10-RL-PS-E4, Sensopart, Germany) to approx. 19 m s<sup>-1</sup>. The generated wave in the incident bar would then result in a strain-rate of 1 000 s<sup>-1</sup>, but due to the stiffness of the sample and the small total deformation required to failure, the incident bar did not have enough time to accelerate to the required speed before the tested

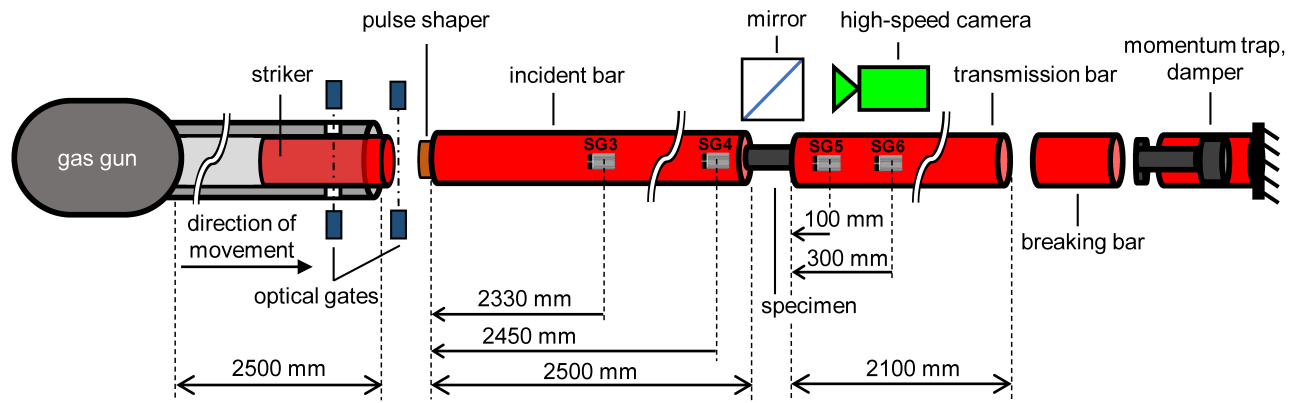


FIGURE 3. The arrangement of the SHPB experimental setup: uni-axial compression with aluminium alloy bars.

specimen disintegrated, and the real strain-rate during the deformation was thus around  $200 \text{ s}^{-1}$  ( $4 \text{ m s}^{-1}$ ). From the trend of the strain-rate curve for the low-rate measurements (green dashed line), an uneven trend can be seen until the breakdown of the sample and the subsequent acceleration up to values of  $1000 \text{ s}^{-1}$ .

The corresponding average stress-strain curve for low-rate (green solid line) shows similar peak stress values to quasi-static loading and only a steeper stress rise. From the calculated deviation of the stress-strain curve marked as a green shadow around the stress-strain curve, it can be concluded that the behaviour is quite uniform throughout the tested set of five specimens.

For the second set of five specimens marked as high-rate (yellow color curves), the speed of the impactor was increased to  $32 \text{ m s}^{-1}$ . As in the previous case, the maximum possible impact velocity was not reached before the sample disintegrated and the deformation rate was roughly  $300 \text{ s}^{-1}$  ( $6 \text{ m s}^{-1}$ ). No significant effect of strain-rate hardening compared to Q-S and low-rate dynamic loading was noted.

The process of the deformation recorded by the high-speed camera can be seen in Figure 4. The upper slide-show consisting of 8 images with a green border corresponds to a low-rate dynamic loading at  $200 \text{ s}^{-1}$ , and similarly the following 8 images with a yellow border correspond to  $300 \text{ s}^{-1}$ .

### 3.2.2. GAP BETWEEN SPECIMEN AND INCIDENT BAR

In this case, a 5 mm gap was left in front of the specimen to solve the problem of insufficient time for the incident bar to accelerate. The incident bar thus gained speed before hitting the specimen. Due to the insufficient number of specimen, only two were tested with this method, namely at the resulting speeds of  $400 \text{ s}^{-1}$  ( $8 \text{ m s}^{-1}$  purple curves) and at  $600 \text{ s}^{-1}$  ( $12 \text{ m s}^{-1}$ , black curves) Figure 5. For the specimen tested at a speed of  $400 \text{ s}^{-1}$ , a similar value of the maximum stress was achieved. The similar response trend according to with the measurement when the sample was in contact with the bars can be seen. A difference in the response trend is only in the gradual build-up of stress, which

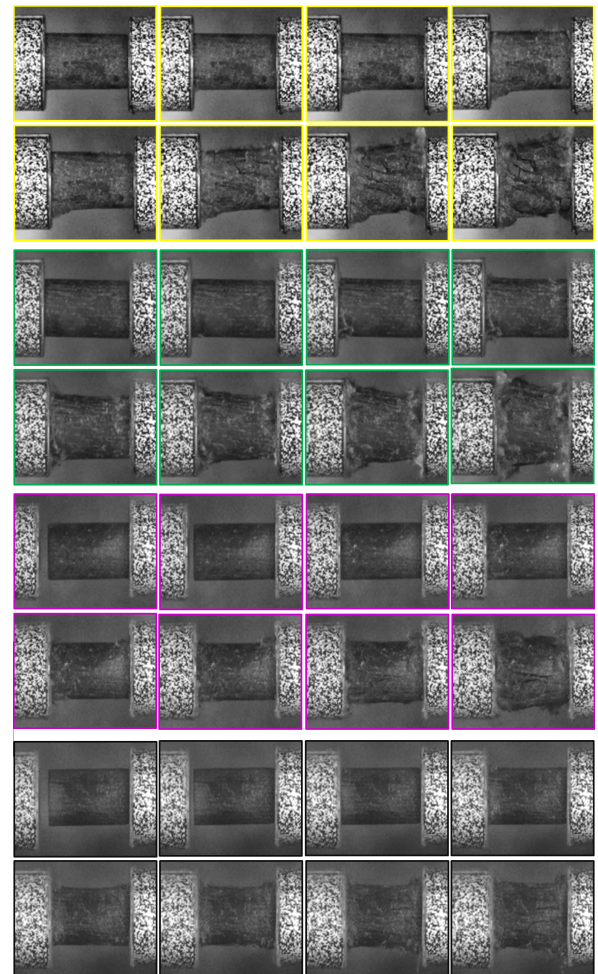


FIGURE 4. Dynamic deformation mechanisms with step of  $17 \mu\text{s}$  between images for the green  $200 \text{ s}^{-1}$  ( $4 \text{ m s}^{-1}$ ), yellow  $300 \text{ s}^{-1}$  ( $6 \text{ m s}^{-1}$ ), purple  $400 \text{ s}^{-1}$  ( $8 \text{ m s}^{-1}$ ), black  $600 \text{ s}^{-1}$  ( $12 \text{ m s}^{-1}$ ).

may be caused by inertial effects caused by the impact of the already accelerated incident bar. The second test with the same arrangement only at a higher speed of  $600 \text{ s}^{-1}$  shows the same stress gradual build-up but only to a value below 250 MPa. Since it is only one specimen, it cannot be concluded that the behaviour of the material has changed, and most likely it is only

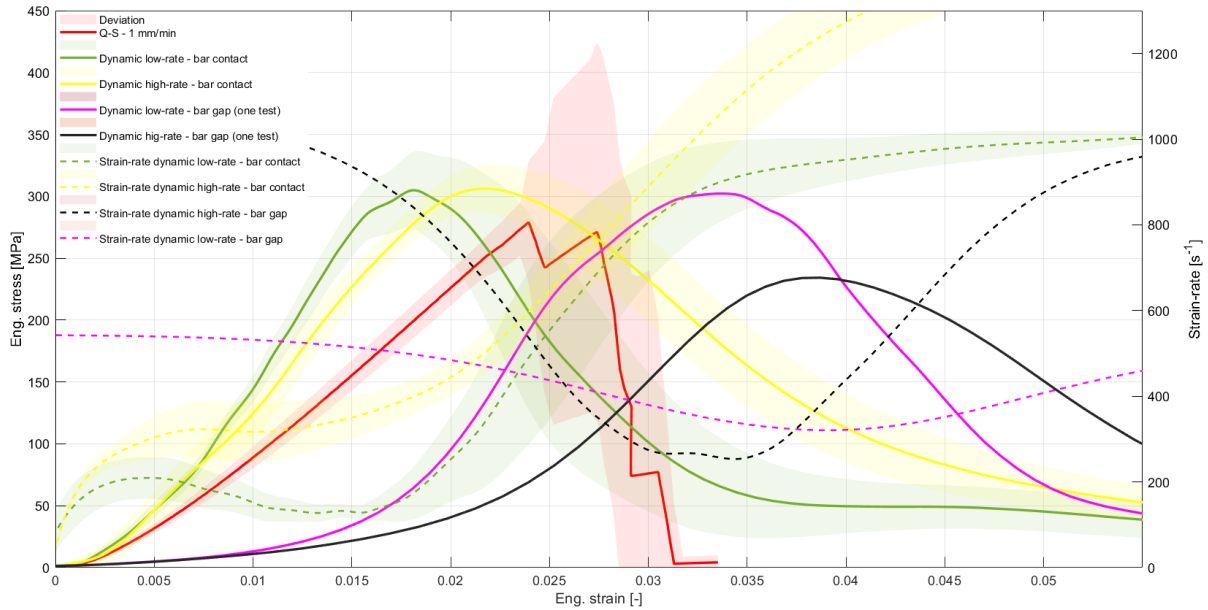


FIGURE 5. Mean stress-strain curves with standard deviation (shadows around curves) for Q-S (red) and dynamic loading with corresponding strain-rate (dashed lines). Green curves –  $200 \text{ s}^{-1}$  ( $4 \text{ m s}^{-1}$ ), yellow curves –  $300 \text{ s}^{-1}$  ( $6 \text{ m s}^{-1}$ ), purple curves –  $400 \text{ s}^{-1}$  ( $8 \text{ m s}^{-1}$ ), black curves –  $600 \text{ s}^{-1}$  ( $12 \text{ m s}^{-1}$ ).

a deviation caused by a different internal structure of the specific tested specimen.

The process of the deformation recorded by the high-speed camera can be seen in Figure 4. The bottom slide-show consisting of 8 images with a black border corresponds to a dynamic load at  $600 \text{ s}^{-1}$ , and similarly the above placed 8 images with a purple border correspond to  $400 \text{ s}^{-1}$ .

### 3.3. DIGITAL IMAGE CORRELATION

DIC is an image processing method that uses tracking and image registration techniques to measure changes in a sequence of images [7]. In this case the modified algorithm of augmented-Lagrangian DIC providing global kinematic compatibility was used [8]. The camera recordings from dynamic experiments were subjected to a DIC analysis to evaluate the captured displacements to describe crack formation and disintegration mechanism.

It was found that in experiments where the specimen is in contact with the incident bar, a crack and subsequent disintegration occur primarily on the incident side and always localized. On the other hand, in both specimens tested with an already accelerated incident bar, crack occurred across the entire width of the sample, and the disintegration also appeared earlier on the back side of the specimen, as can be seen in selected images Figure 6.

## 4. CONCLUSIONS

A description of the fundamental mechanical behaviour of the basalt rock specimens was determined from quasi-static uni-axial compression tests. To assess the strain-rate sensitivity of the mechanical re-

sponse, dynamic compression experiments at four different loading-rates and two different loading modes using the SHPB apparatus were conducted. Optical measurement methods employing a high-speed camera were applied. DIC algorithm was used to evaluate the displacements fields from the camera recordings to investigated failure mechanism under applied loads. Based on the results obtained from the experimental investigations, it is possible to conclude:

- A strain-rate sensitivity of the deformation behaviour of the investigated basalt rock was not indicated. The decrease in recorded values of stress occurred for last specimen at  $600 \text{ s}^{-1}$  was not conclusive and more specimens need to be tested for sufficient statistics.
- The starting part of the trend of stress-strain curves was different for two modes of loading (bar in contact and with gap) probably due to inertia effect of bars. This phenomena could be investigated with DIC evaluation on both end of the bar and evaluation of their velocities during the test.
- Loading mode with gap at the front of the specimen seems promising as a method for dynamic testing of tough materials with low deformation around few percent as its creates the possibility to reach higher strain-rates. To clearly describe the effect of such a loading mode compared to the standard placement, it is necessary to perform a larger statistically significant set of measurements and, if possible, include the evaluation of the velocity of both ends of the bars near the specimen using DIC.

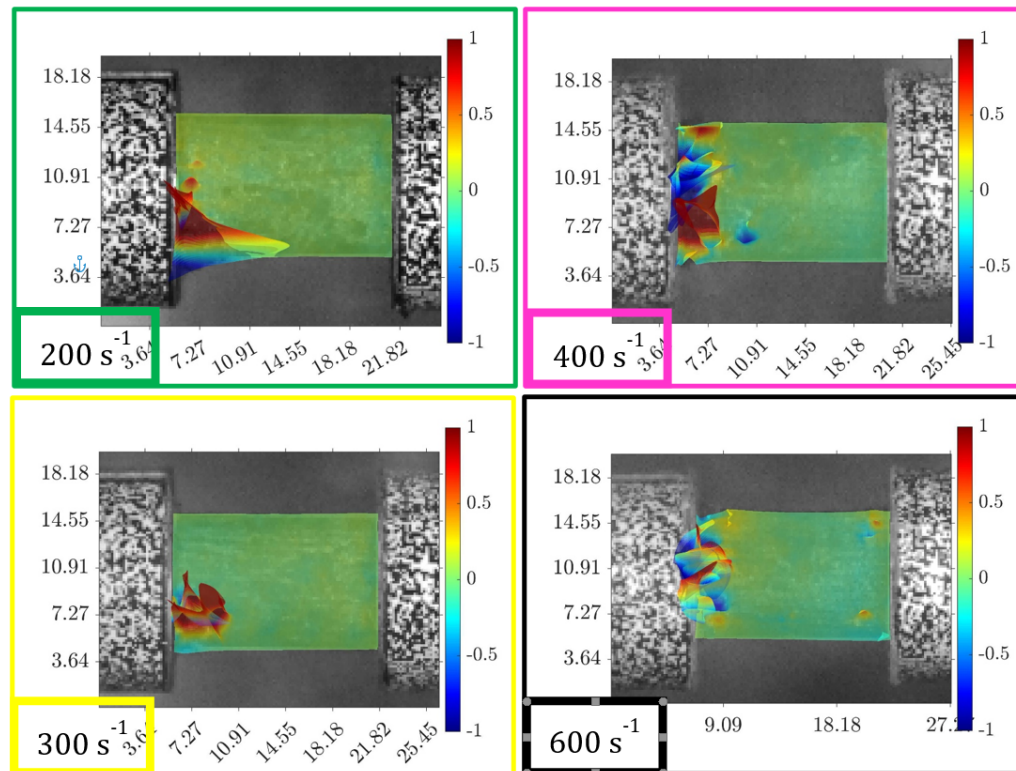


FIGURE 6. Displacement fields for selected specimens taken at the beginning of the disintegration process.

#### ACKNOWLEDGEMENTS

This research was funded by Czech Science Foundation (project Junior Star no. 22-18033M) and by the Grant Agency of the Czech Technical University in Prague, grant No. SGS23/134/OHK2/2T/16. The conference participation was supported by Czech National IMEKO Committee.

#### REFERENCES

- [1] M. Vyhliđal, I. Rozsypalova, H. řimonova, et al. Influence of rock inclusion composition on the fracture response of cement-based composite specimens. *Procedia Structural Integrity* **33**:966–981, 2021. <https://doi.org/10.1016/j.prostr.2021.10.107>
- [2] M. Vyhliđal, I. Rozsypalova, H. řimonova, et al. Effect of petrographic composition and chemistry of aggregate on the local and general fracture response of cementitious composites. *Frattura ed Integrita Strutturale* **16**(60):13–29, 2022. <https://doi.org/10.3221/igf-esis.60.02>
- [3] P.-C. Aitcin. *High performance concrete*. CRC press, 1998.
- [4] A. M. Neville, et al. *Properties of concrete*, vol. 4. Longman London, 1995.
- [5] D. Lange-Kornbak, B. Karihaloo. Fracture mechanical prediction of transitional failure and strength of singly-reinforced beams. In *Minimum Reinforcement in Concrete Members*, pp. 31–66. Elsevier, 1999. [https://doi.org/10.1016/s1566-1369\(99\)80061-2](https://doi.org/10.1016/s1566-1369(99)80061-2)
- [6] V. Slivka, M. Vavro. The significance of textural and structural properties of North-Moravian basaltoids for the manufacture of mineral fibres. *Ceramics Silikaty* **40**(4):149–159, 1996.
- [7] N. Novak, D. Kytyr, V. Rada, et al. Compression behaviour of TPMS-filled stainless steel tubes. *Materials Science and Engineering: A* **852**:143680, 2022. <https://doi.org/10.1016/j.msea.2022.143680>
- [8] J. Yang, K. Bhattacharya. Augmented Lagrangian digital image correlation. *Experimental Mechanics* **59**(2):187–205, 2018. <https://doi.org/10.1007/s11340-018-00457-0>